https://doi.org/10.18321/ectj976

Comparative Analysis of Physicochemical Properties of Rutile TiO_2 with Hierarchical 3D Architecture Prepared by Liquid Hydrolysis of $TiCl_4$ and Hydrothermal Method

N.V. Shikina[1]*, S.A. Yashnik[1], A.V. Toktarev[1], A.V. Ishchenko[1], V.A. Ushakov[1], M.S. Mel'gunov[1], Z.A. Mansurov[3], Z.R. Ismagilov[1,2]

[1]Federal Research Center Boreskov Institute of Catalysis SB RAS, 5 pr. Akad. Lavrentieva, Novosibirsk, Russia
[2]Federal Research Center of Coal and Coal Chemistry Institute of Coal Chemistry and Materials Science SB RAS, 18 Sovetskiy pr., Kemerovo, Russia
[3]Institute of Combustion Problems, 172 Bogenbay Batyr str., Almaty, Kazakhstan

Article info

Received:
5 February 2020

Received in revised form:
18 March 2020

Accepted:
25 April 2020

Keywords:
Titanium dioxide
Nanostructured rutile
Porous structure
Thermal treatment

Abstract

TiO_2 (rutile) samples with a hierarchical 3D nanostructure of the particles were synthesized by two methods: liquid hydrolysis of $TiCl_4$ at 90 °C and atmospheric pressure; hydrothermal synthesis from $TiCl_4$ at 160 °C and different $[H_2O]/[Ti]$ ratios. The effect exerted by conditions of the synthesis and post-treatments on the crystallite size, morphology, electronic properties and pore structure of the rutile samples was investigated. It was shown that severe hydrothermal conditions with the ratio $[H_2O]/[Ti]$ = 20 provide the formation of a more perfect crystal structure of rutile with a smaller band gap energy (3.00 eV against 3.06 eV for the rutile obtained by liquid hydrolysis at atmospheric pressure). The study revealed the stabilizing effect of cerium cations on the pore structure of rutile, which changes upon thermal treatment.

1. Introduction

Different morphological types of hierarchical 3D nanostructures (HNSs) form a new class of materials for various applications. Porous three-dimensional interconnected structures are characterized by large surface-to-volume ratios, which provide additional possibilities for the occurrence of catalytic reactions within the framework [1]. In recent years, the study of TiO_2 HNSs has been a hot topic in the field of photocatalysis and photocatalytic materials for energy and environmental applications [1–4]. The prospects of TiO_2 HNSs for the photocatalytic processes are related to the combination of TiO_2 benefits including non-toxicity, chemical stability, and electronic configuration with a hierarchical structure, which provides an extended and accessible surface.

*Corresponding author. E-mail: shikina@catalysis.ru

TiO_2 is a semiconductor with an energy band gap (E_g) between the filled valence band (VB) and an empty conduction band (CB) equal to 3.0 and 3.2 eV for rutile and anatase crystal phases, respectively [5]. When TiO_2 is exposed to light having photon energy exceeding the band gap, $h\nu > E_g$, electrons are excited from VB to CB, leaving electron vacancies (i.e. holes) in VB [6–8]. The photogenerated electrons and holes can migrate to the TiO_2 surface and participate in surface redox reactions. The high redox potential of generated holes and the formation of reactive oxidants, resulting from the interaction of generated electrons with surface oxygen, provide an effective degradation of various organic pollutants absorbed on the TiO_2 surface [9, 10].

Rutile TiO_2 is characterized by a relatively small band gap (as compared to other semiconductors), and an improvement in the material design by forming the hierarchical nanostructures opens

up wide possibilities for its use in photocatalysis due to high specific surface area, beneficial light absorption, and appropriate refractive index, along with other excellent physical and chemical properties [11–13]. The properties of a hierarchical system are determined mostly by the properties of agglomerated particles, their packing and morphology, i.e. the texture of the material. Hierarchical nanostructured materials, which possess the porous structure of multiscale porosities on different pore diameters from micro-, meso- to macropores, are much desired to present the synergistic attractive advantages of each scale of hierarchical pores in the development of catalysis, adsorption, separation, energy, photocatalysis and biochemistry [14]. The crystal structure is formed in the synthesis step; so the chosen strategy of the synthesis commonly determines the crystallinity, morphology and textural properties of the material, as well as its electronic properties. Among various methods used to synthesize rutile TiO_2 HNSs: hydrothermal method, solvothermal method, microwave treatment, pulsed laser deposition, anodization, photolithography, vapor deposition and others, the hydrothermal synthesis is the most used one. As the name indicates, the method involves heating in an aqueous medium in the closed volume of the reactor, which leads to a pressure boost during the synthesis. Generally, sealed Teflon-lined steel autoclaves are used under controlled temperature and pressure conditions. This process is mainly used for the preparation of small-sized particles for achieving enhanced surface area. The morphology of the particles can be varied by changing crystallization temperature, time and concentration of etching chemicals [15].

Only a few works are devoted to the synthesis of rutile TiO_2 HNSs by hydrolysis at atmospheric pressure [16–19]. This method makes it possible to achieve a very high specific surface area (up to 200 m^2/g); however, the synthesized material has a large amount of structural defects, which can enhance its photocatalytic activity [20], on the one hand, but diminish the stability of its properties, on the other hand.

It is often necessary to carry out calcination of the material for its further application, in particular, in catalytic processes. The enhancement of thermal stability of the material is a topical task because textural characteristics of nanostructured rutile are of key importance for its application as a support of catalysts or photocatalysts. It is known that the stabilization of the structural and dispersed properties of materials is facilitated by the introduction of various modifying additives into their composition. In [21–23], titania was modified with cations of different metals for shifting the anatase → rutile polymorphous transformations to higher temperatures, which is reached by inhibiting the growth of crystallites stabilized by CeO_2 [21], SiO_2 [22] or Y_2O_3 [23] interlayers. Such modification results in the formation of the nanocrystalline anatase structure comprising incoherently intergrown particles, and significantly hinders the growth of anatase crystallites to the critical values at which anatase converts to rutile. In [24, 25], it was found that modification with La and Ce ions [24] or La and Mg ions [25] stabilizes the alumina pore structure and specific surface area. The authors revealed a relation between the effect exerted by metal cations on polymorphous transformations in alumina and its structural-mechanical properties. The introduction of 3–10 wt.% Ce into the rutile matrix was shown in [26] to decrease the growth of nanorutile crystallites under the action of high temperature (300–1000 °C) and provide the formation of a more porous structure in comparison with unmodified samples.

It is possible that rutile samples obtained under mild hydrolysis conditions at atmospheric pressure will be more vulnerable to thermal post-treatment in comparison with the material obtained under hydrothermal conditions. Comparative data on the properties of rutile samples synthesized under different conditions but having a similar morphology are absent in the literature. A comparison of the properties of materials based on the published data will not be correct because the reported studies are often performed with different precursors and details of the synthesis (concentration of reagents, pH of the medium, reagents from different manufacturers, and equipment). The aim of this work is a comparative analysis of structural, textural, morphological and electronic properties of the samples of hierarchical 3D nanostructured rutile obtained by hydrolysis of $TiCl_4$ at atmospheric pressure and by hydrothermal synthesis; thermal stability of materials in the temperature range of 300–1000 °C and the possibility to stabilize textural characteristics by introducing cerium cations are also investigated.

2. Materials and methods

2.1. Synthesis of TiO_2 materials

Rutile synthesis by liquid hydrolysis of $TiCl_4$.

The method employed for the synthesis of nanostructured rutile is described in detail in [19]. Briefly, titania (rutile) was synthesized by the sol-gel method via the hydrolysis of titanium tetrachloride in distilled water at the molar ratios $[Cl^-]/[Ti^{4+}] = 4$ and $[H_2O]/[Ti^{4+}] = 39$. The hydrolysis reaction was carried out in a thermostatically controlled glass reactor at 90 °C for 5 h under continuous stirring. The white suspension was then cooled to room temperature and aged for 24 h. After that, the resulting suspension was separated into sediment and mother liquor by decantation. The impurities, which are mostly the chloride ions, were removed by dialysis against distilled water. After that, the sediment was dried at 100 °C in air and calcined at 300, 500, 700 and 1000 °C. The samples are designated as R90/T, where R is rutile and 90 is the temperature of $TiCl_4$ hydrolysis. T is the calcination temperature.

2.1.1. Post-treatment of rutile under hydrothermal conditions

A part of the sample from the reactor (before the decantation stage) was placed in a Teflon shell and heated in an autoclave for 2 h at 160 °C. After that, the suspension was cooled to room temperature and treated, dried and calcined in the same manner as after the hydrolysis procedure. The samples are designated as R90-160/T, where R is rutile, 90 and 160 are the temperatures of $TiCl_4$ hydrolysis and hydrothermal treatment. T is the calcination temperature.

2.1.2. Rutile synthesis by hydrothermal method

The required amount of the $TiCl_4$ sample was supplemented with water and stirred on an ice bath for 30 min; the mixture was then transferred into a Teflon shell and heated in an autoclave for 2 h at 160 °C. In the first experiment, molar ratios of reagents were $[Cl^-]/[Ti^{4+}] = 4$ and $[H_2O]/[Ti^{4+}] = 39$ (the sample is designated as R160(40)), while in the second one, $[Cl^-]/[Ti^{4+}] = 4$ and $[H_2O]/[Ti^{4+}] = 20$ (the samples are designated as R160(20). After that, the suspensions were cooled to room temperature and then treated, dried and calcined as after the hydrolysis procedure. In the designation of the R160(20)/T or R160(40)/T sample, T indicates the calcination temperature.

2.1.3. Modification of rutile with 5% CeO_2

The air-dried (not calcined) samples R90 and R160(20) were impregnated with a $Ce(NO_3)_3 \cdot 6H_2O$ aqueous solution by incipient wetness method with subsequent drying at 80 °C (5Ce/R90 and 5Ce/R160(20) samples, where 5 is the weight fraction (%) of CeO_2 in the sample). For comparison, the R90 sample was modified with cerium under hydrothermal conditions. To this end, the sample was poured with a $Ce(NO_3)_3 \cdot 6H_2O$ aqueous solution and heated in an autoclave for 2 h at 160 °C; after cooling and separation of mother liquor, the sample was dried under a lamp at 100 °C. The content of CeO_2 in rutile was 2%, the rest was in mother liquor (the 2Ce160/R90 sample). The modified samples were calcined at 500 and 700 °C.

2.2. Investigation of physicochemical properties

The chemical composition of the synthesized samples was estimated by inductively coupled plasma atomic emission spectroscopy on an Optima 4300 DV instrument and by X-ray fluorescence analysis on an ARL-Advant'x analyzer with an Rh-anode X-ray tube.

XRD studies were performed using an HZG-4C (Freiberger Präzisionsmechanik) X-ray diffractometer with a CoK_α monochromatic source (λ = 1.79021 Å) in a continuous mode in the 2θ angular range from 20 to 85°. Crystallite sizes were estimated using the Scherrer equation.

Textural properties (specific surface area and pore volume) were analyzed by low-temperature nitrogen adsorption (ASAP-2400, Micromeritics).

Transmission electron microscopy (TEM) and high resolution transmission electron microscopy (HR-TEM) images were obtained using a JEM-2010 (JEOL, Japan) microscope.

UV-Vis diffuse reflectance spectra were recorded at room temperature in the range of 200–900 nm with 1 nm resolution using a Shimadzu UV-2501 PC spectrophotometer equipped with an IRS-240 A diffuse reflectance attachment. A special pre-packed $BaSO_4$ was used as a reflectance standard. UV-Vis spectra were recalculated in the Kubelka-Munk coordinates as follows:

$$F(R_\infty) = \frac{(1 - R_\infty/100)^2}{2R_\infty/100}$$

where R_∞ is the reflectance (%). The optical band gap for the rutile samples was estimated using the Tauc method [27] by plotting $(F(R_\infty)h\nu)^2$ versus hν and $(F(R_\infty)h\nu)^{1/2}$ versus hν, and their linear extrapolation to intercept the energy axis.

3. Results and discussion

3.1. Crystal structure and crystallite size

The phase composition and crystallite size of the samples obtained by hydrolysis at atmospheric pressure and under hydrothermal conditions were investigated by XRD. According to the diffraction patterns (Fig. 1), all the samples, irrespective of the synthesis method, have peaks at 2θ angles 32.00, 42.19, 48.30, 64.07 and 74.45° corresponding to the rutile phase. The average size of crystallites calculated by the Scherrer formula depends on the synthesis method. The uncalcined rutile sample (R90) obtained by hydrolysis at atmospheric pressure has the smallest crystallite size along all crystallographic directions (Table 1, sample 1). Post-treatment of this sample under hydrothermal conditions at 160 °C (sample 6 – R90-160) does not alter the crystal structure of TiO_2, but increases the size of crystallites. A similar result is reached when rutile is obtained by hydrothermal synthesis from $TiCl_4$ at different $[H_2O]/[Ti^{4+}]$ ratios (Table 1, samples 11 and 16 – R160(40) and R160(20)). Therewith, the $[H_2O]/[Ti^{4+}]$ ratio in hydrothermal synthesis and the succession of hydrothermal treatment (immediately or after the formation of rutile phase at atmospheric pressure) exert virtually no effect on the size of the rutile crystallites.

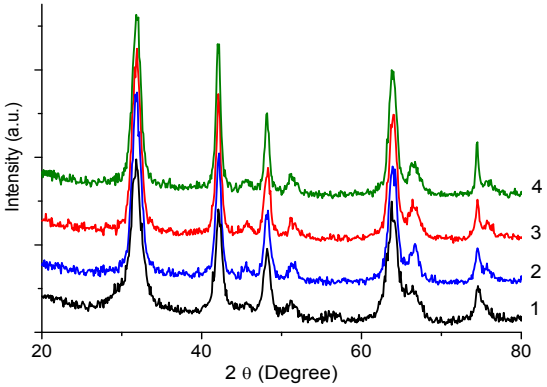

Fig. 1. XRD patterns of the TiO_2 samples prepared by: 1 – liquid hydrolysis of $TiCl_4$ (sample R90); 2 – post-treatment of R90 under hydrothermal condition at 160 °C (sample R90-160); 3 and 4 – hydrothermal method at 160 °C (samples R160(40) and R160(20), respectively).

Table 1
Effect of the calcination temperature on the crystallite size of the rutile samples synthesized by liquid hydrolysis of $TiCl_4$ and hydrothermal method

#	Samples	$T_{calc.}$, °C	Crystallite size (Å) along crystallographic directions				
			110 (32.00°)	101 (42.19°)	111 (48.30°)	211 (64.07°)	002 (74.45°)
1	R90	100	85	150	160	90	90
2		300	160	220	210	160	230
3		500	220	250	250	180	200
4		700	>250	>250	>250	>250	>250
5		1000	>250	>250	>250	>250	>250
6	R90-160	100	95	175	165	125	>300
7		300	120	170	170	120	130
8		500	220	220	250	220	250
9		700	>500	>500	>500	>500	>500
10		1000	>500	>500	>500	>500	>500
11	R160(40)	100	95	230	165	125	>300
12		300	120	170	220	130	130
13		500	250	>300	>300	250	>500
14		700	>500	>500	>500	>500	>500
15		1000	>500	>500	>500	>500	>500
16	R160(20)	100	95	230	230	125	>300
17		300	160	220	220	140	220
18		500	300	500	300	300	500
19		700	>500	>500	>500	>500	>500
20		1000	>500	>500	>500	>500	>500

Table 2
Effect of the Ce cations introduction on the crystallite size of the rutile samples synthesized by liquid hydrolysis of $TiCl_4$ and hydrothermal method

Samples	$T_{calc.}$, °C	Crystallite size (Å) along crystallographic directions				
		110 (32.00°)	101 (42.19°)	111 (48.30°)	211 (64.07°)	002 (74.45°)
5Ce/R90	500	120	200	150	115	150
	700	160	240	250	180	200
2Ce160/R90	500	150	220	200	170	240
	700	250	250	250	250	250
5Ce/R160(20)	500	160	>250	>250	170	>250
	700	200	>250	>250	>250	>250

The size of rutile crystallites increases upon thermal treatment for all the samples irrespective of the initial conditions of their synthesis. Thus, calcination at 300 °C increases the crystallite size mostly for the R90 sample. At 500 °C, an increase in the crystallite size is most pronounced for the R160(40) and R160(20) samples that were obtained directly by hydrothermal method; depending on crystallographic direction, their size is in the range of 250–500 Å, whereas the crystallite size of R90 and R90-160 samples does not exceed 250 Å. A further elevation of the calcination temperature leads to even stronger growth of rutile crystallites; therewith, the crystallite size of the R90 sample is two times smaller as compared to the samples subjected to hydrothermal post-treatment or initially synthesized under hydrothermal conditions. Thus, it can be concluded that the synthesis performed under more severe hydrothermal conditions in comparison with the hydrolysis at atmospheric pressure enhances the thermal stability of rutile only up to 300 °C, whereas a further increase in temperature results in the formation of large crystallites with the size above 500 Å.

Modification of uncalcined rutile samples with cerium cations hinders the growth of crystallites upon calcination (Table 2). Most efficient is the introduction of cerium by incipient wetness impregnation (5Ce/R90 and 5Ce/R160(20) samples). The stabilizing effect of cerium introduction in the R90 sample under hydrothermal conditions (the 2Ce160/R90 sample) is observed upon calcination of the sample at 500 °C, while at 700 °C this effect is insignificant.

3.2. Textural properties

Investigation of the textural properties of rutile samples by the low-temperature nitrogen adsorption demonstrated that the sample obtained at atmospheric pressure has a more developed specific surface area as compared to hydrothermal samples. Specific surface areas for the uncalcined samples R90, R90-160, R160(40) and R160(20) are 170, 89, 100 and 65, respectively. Specific surface area and total pore volume of the samples were shown to decrease upon calcination at 300–1000 °C. The decrease in specific surface area is virtually independent of the rutile synthesis conditions (Fig. 2a). The pore volume (V_{pore}) of the calcined samples decreases not so dramatically as their specific surface area (Fig. 2b), and the dynamics of the V_{pore} decrease for R90 sample differs from that observed for hydrothermal samples. This sample has a virtually constant total pore volume up to a temperature of 500 °C. As the calcination temperature is raised, the pore volume values remain constant, whereas the specific surface area decreases and the average pore size increases; this testifies to implementation of the surface-diffusion sintering mechanism in the temperature range of 300–500 °C [20]. For samples R160(40) and R160(20), sintering follows the volume-diffusion mechanism, whereas for the R90-160 sample subjected to hydrothermal post-treatment, sintering proceeds most likely by the mixed mechanism.

The introduction of cerium cations in the rutile matrix made it possible to hinder the decrease in specific surface area due to the formation of smaller crystallites in comparison with pristine rutile, as was shown by XRD. Ceria was introduced into rutile (R90) by two methods: conventional incipient wetness (dry) impregnation at atmospheric pressure and that in an excess of the solution under hydrothermal conditions. In the first case, rutile contained ca. 5% of CeO_2 (5Ce/R90), while in the second case, only 2% (2Ce160/R90); however, even such a low content was sufficient to produce the stabilizing effect (Fig. 3a and b), although here it was much less pronounced than in the first case.

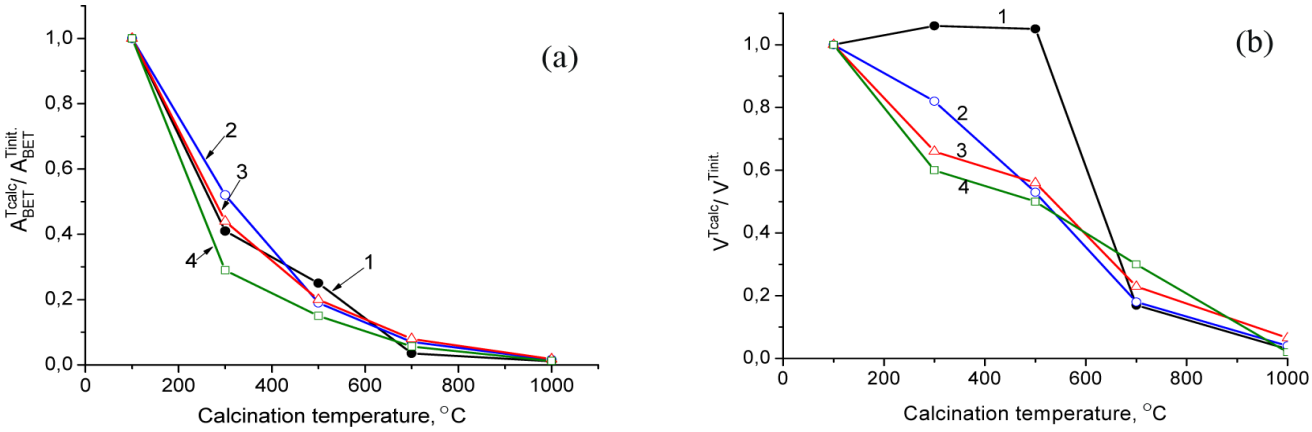

Fig. 2. A decrease in specific surface area (a) and total pore volume (b) of the calcined rutile samples with respect to the initial values for uncalcined (as synthesized) samples: 1 – R90, 2 – R90-160, 3 – R160(40), 4 – 160(20).

The stabilizing effect of cerium cations at a temperature of 500 °C (Fig. 3a) is connected with the formation of a more fine-pored structure as compared to unmodified sample, while at 700 °C – with the formation of a greater amount of both fine and wide pores (Fig. 3b). When cerium is introduced in the R160(20) sample by incipient wetness (dry) impregnation, the stabilizing effect is more pronounced for the samples calcined at 500 °C. In this case, the formation of a more fine-pored structure (Fig. 4a) than in pristine rutile is observed. At 700 °C, modification with cerium increases only the amount of wide pores with a diameter greater than 30 nm (Fig. 4b); in this case, specific surface areas of pristine and modified rutile are virtually similar.

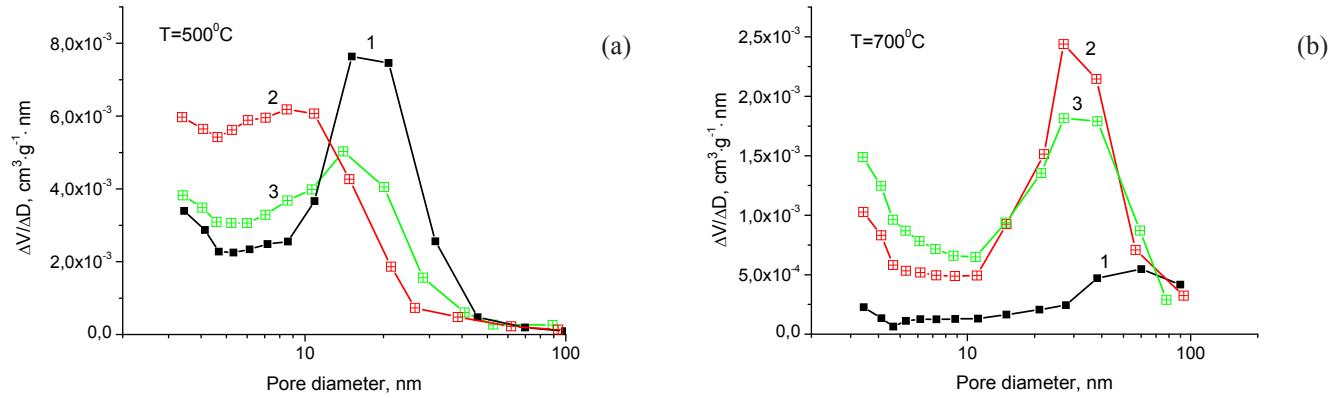

Fig. 3. Differential pore size distribution in the rutile samples calcined at 500 (a) and 700 °C (b): 1 – unmodified R90; 2 – 5Ce/R90 modified with cerium at atmospheric pressure; 3 – 2Ce160/R90 modified with cerium under hydrothermal conditions.

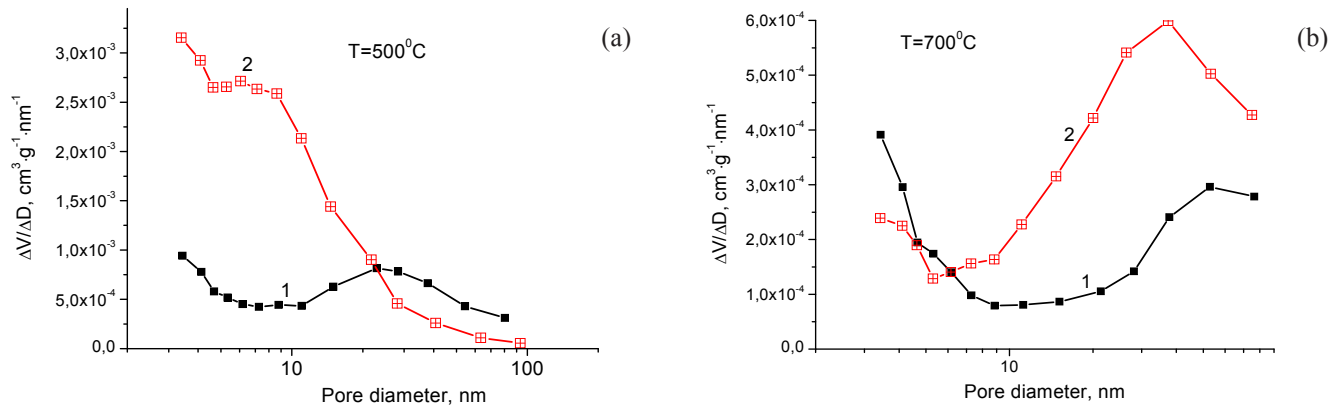

Fig. 4. Differential pore size distribution in the rutile samples calcined at 500 (a) and 700 °C (b): 1 – unmodified R160(20); 2 – 5Ce/R160(20) modified with cerium.

3.3. Morphology of materials

Particles of the material obtained by $TiCl_4$ hydrolysis belong to the rutile phase and have an intricate packing system; their characteristics correspond to those of 3D hierarchical structures. At the first structural level, the primary particles coherently intergrow to form nanowires. The oriented addition of the primary particles includes spontaneous self-organization of adjacent particles, due to which they become involved in the joint crystallographic orientation with the subsequent agglomeration of the particles at the plane interface [28]. Binding of the particles decreases the total energy of their aggregates due to the surface energy of uncompensated bonds of primary particles, thus leading to the coherent intergrowth of particles that is more advantageous in terms of energy. Nanowires forming the first structural level (Fig. 5a–c) are joined into the fan-shaped aggregates (Fig. 5d–f) that constitute the second structural level. At the third level, the aggregates merge into large spherical 3D particles (Fig. 5g–i).

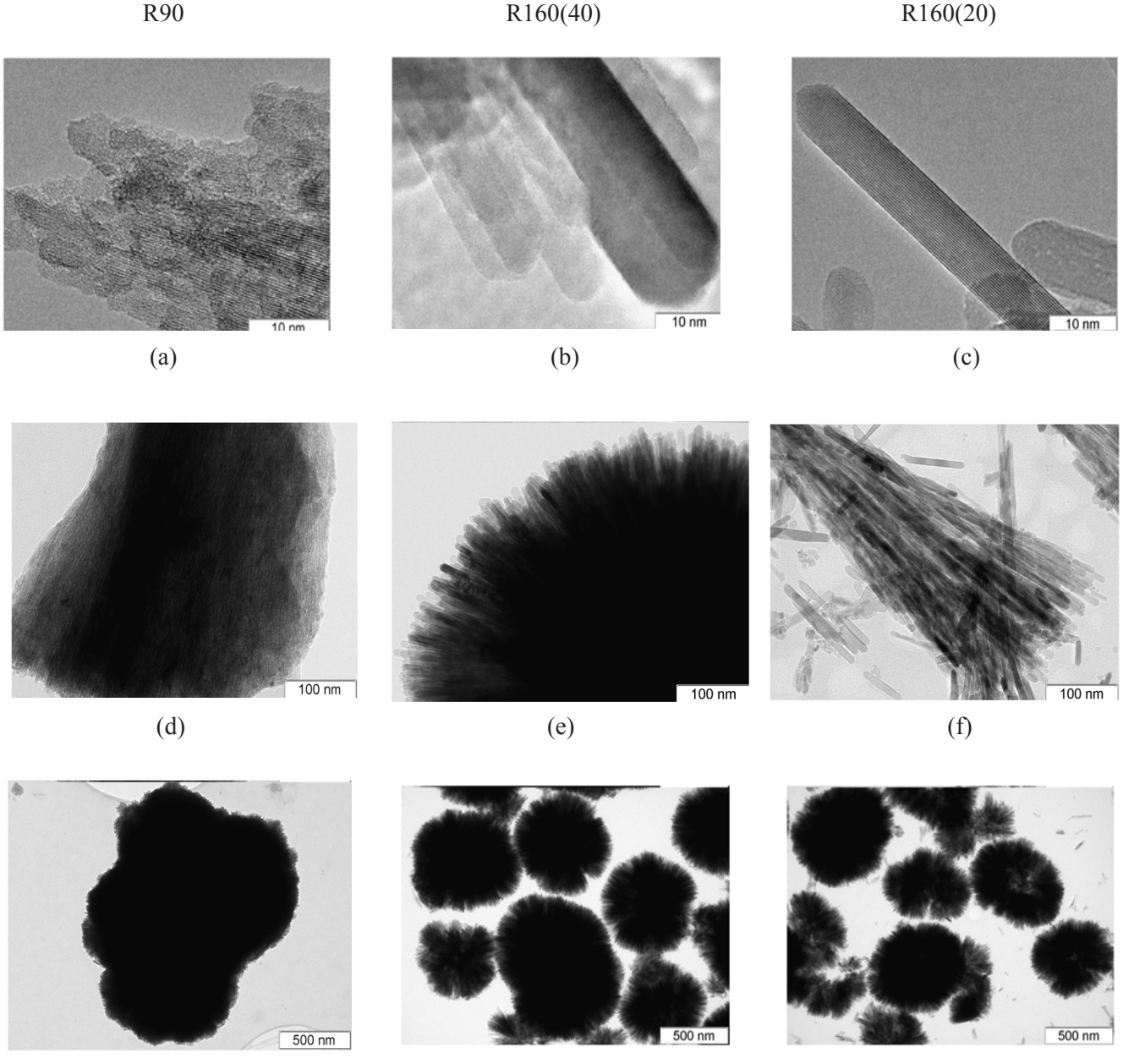

Fig. 5. HRTEM images of rutile crystallites and TEM images of the aggregates of particles in uncalcined rutile samples obtained at atmospheric pressure: (a), (d), (g) – R90; and under hydrothermal conditions: (b), (e), (h) – R160(40); (c), (f), (i) – R160(20)

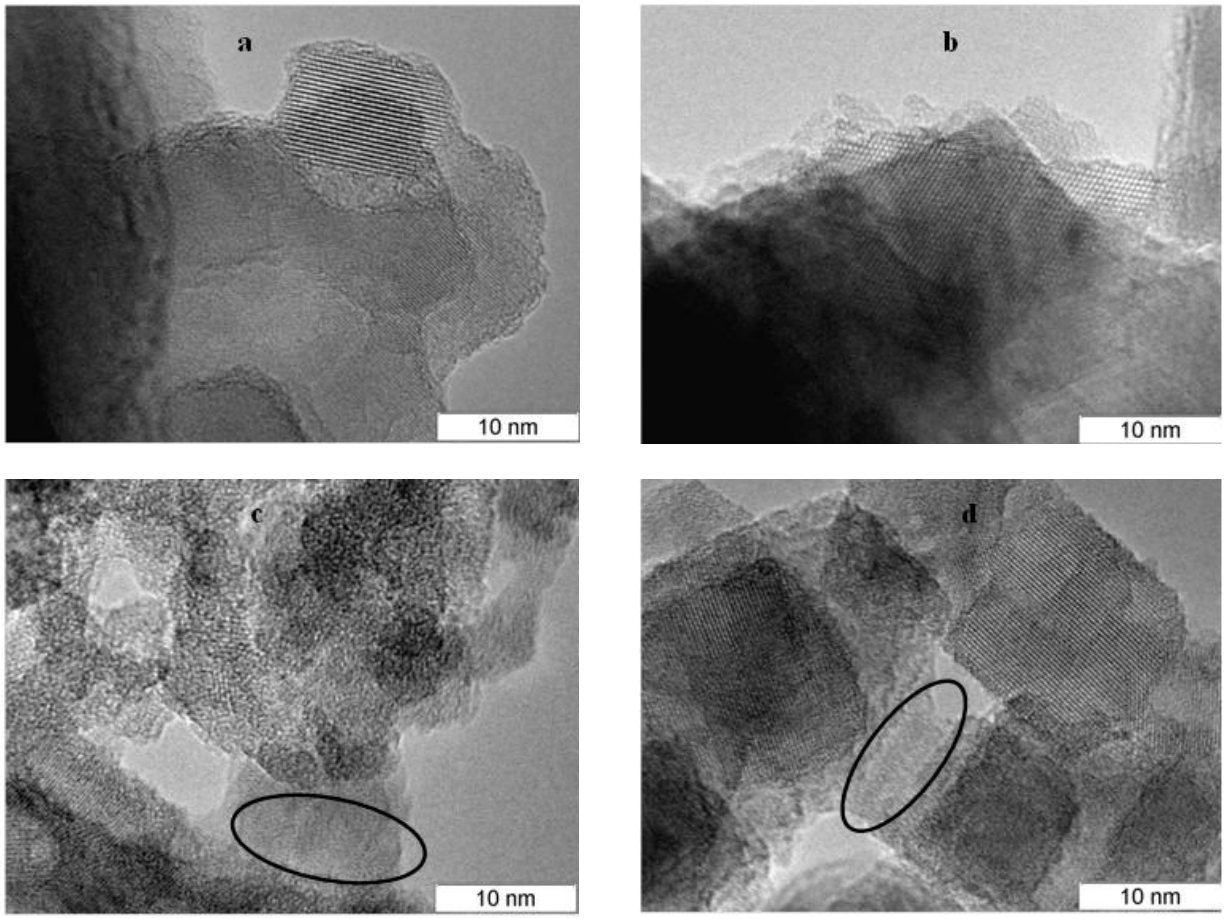

Fig. 6. TEM images of R90 samples calcined at 500 (a) and 700 °C (b); 5Ce/R90 calcined at 500 (c) and 700 °C (d).

According to TEM studies, hydrothermal samples are more crystallized (Fig. 5b–c) and less defect than the rutile sample R90 synthesized at atmospheric pressure (Fig. 5a). The highest degree of crystallization is observed for the R160(20) sample, which was synthesized at lower $[H_2O]/[Ti^{4+}]$ ratios (Fig. 5c). The more severe are the synthesis conditions, the more perfect is the resulting crystal structure. According to XRD, the thickness of filamentary crystallites in fan-shaped aggregates for hydrothermal samples (Fig. 5e and f) exceeds nearly twofold the thickness of filaments in the R90 sample (Fig. 5d). Spherical 3D structures of hydrothermal samples are more compact and have a more uniform size distribution as compared to the R90 sample, which was synthesized under mild conditions at atmospheric pressure (Fig. 5g–i).

The morphological evolution of pristine and cerium-doped rutile samples upon thermal treatment was monitored using R90 and 5Ce/R90 samples. Fig. 6 displays TEM images of the rutile samples calcined at 500 and 700 °C.

According to TEM data, the intergrowth of crystallites at the interblock boundaries is observed in pristine rutile samples at 500 °C (Fig. 6a) and 700 °C (Fig. 6b). A different pattern is obtained for the rutile sample modified with 5% CeO_2 (Fig. 6c and d). Between rutile particles, there are interlayers of the weakly crystallized cerium compound (Fig. 6d, outlined with an oval), which prevents the intergrowth of rutile crystallites at the interblock boundaries and forms the porous structure of the material. It should be noted that the crystallized ceria phase is not detected by XRD in the samples calcined at 500 and 700 °C. Titania may inhibit the crystallization of ceria, which concentrates in the region of interblock boundaries of rutile in the amorphous state.

3.4. Electronic properties of materials

The UV absorption spectrum of TiO_2 nanoparticles can be used to estimate the band gap energy (E_g) from its fundamental absorption edge, the sole band present in the electronic diffuse reflectance spectra of TiO_2. As seen in Fig. 7, this intense absorption occurs in the spectral region below 410 nm irrespective of the rutile synthesis method.

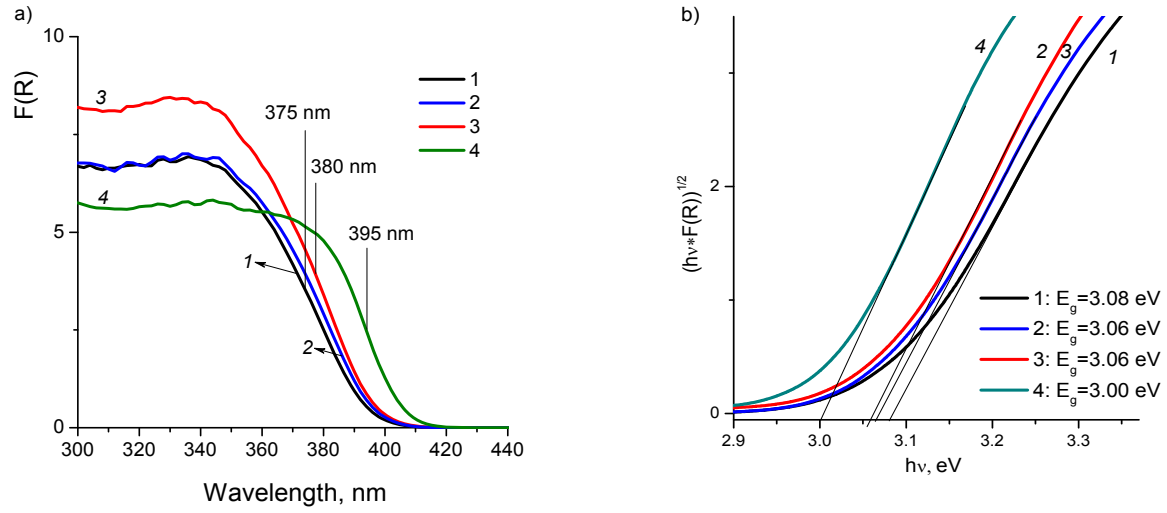

Fig. 7. UV-Vis DR spectra (a) and their linearization in coordinates $(h\nu*F(R_\infty))^{1/2}$ vrs hν for graphical determination of the band gap energy for rutile samples in dependence on the synthesis method: 1 – R90; 2 – R90-160; 3 – R160(40); 4 – 160(20).

The form, energy and intensity of absorption were virtually identical for the TiO_2 samples obtained by hydrolysis at atmospheric pressure with or without treatment under hydrothermal conditions at 160 °C. This is caused by a similar phase composition of the sample and close crystallographic sizes of its particles. Electronic spectra of the R160(20) and R160(40) samples obtained under hydrothermal conditions are shifted toward higher wavelengths. Note that the absorption edge energy of the sample is affected to a greater extent by the $[H_2O]/[Ti^{4+}]$ ratio used in the synthesis. It was equal to 395 and 380 nm for R160(20) and R160(40) samples, respectively. The revealed shift of the absorption band edge was caused by the difference in the size of TiO_2 particles and probably also by a more perfect crystal arrangement of the rutile particles obtained under hydrothermal conditions at $[H_2O]/[Ti^{4+}] = 20$.

The band gap widths calculated for the rutile sample R90, which was synthesized at atmospheric pressure, and for the R160(20) sample, which was synthesized under severe hydrothermal conditions, were equal to 3.08 and 3.00 eV, respectively. Such changes in the electronic properties may be attributed to structural differences in the materials (for example, structural defects) and particle sizes, which are likely to affect their photocatalytic properties. The E_g values for anatase and rutile TiO_2 are in the range of 3.20–3.57 [29–31] and 3.02–3.23 eV [29, 31], respectively, but strongly depend on the particle size and morphology [29, 32] and the doping cation [31, 33, 34]. A comparison of experimental data with the literature data shows that the band gap energy for the TiO_2 particles obtained in our study corresponds to the range determined for rutile. Experimental data on E_g for R90 and R160(20) samples well agree with the established fact that the band gap width decreases with increasing the TiO_2 particle size [32].

The band gap E_g is an important characteristic of a semiconductor for its application in optics and photocatalysis. For the photocatalytic application of titanium dioxide, it is known that the smaller is the band gap energy, the more efficient is the absorption of solar energy by the sample. On the other hand, high E_g values provide advantages for applying the material as a dielectric in electronic devices and light pipes.

4. Conclusion

XRD, BET, TEM and UV-Vis DR methods were used for comparative analysis of physicochemical properties of TiO_2 (rutile) having a hierarchical 3D structure, which was synthesized at 90 °C and atmospheric pressure or under the conditions of hydrothermal synthesis at 160 °C. It was shown that mild conditions of the synthesis lead to the formation of smaller rutile crystallites with low crystallinity and high specific surface area as compared to hydrothermal conditions.

Thermal treatment at 300–1000 °C results in the growth of rutile crystallites along all crystallographic directions irrespective of the synthesis conditions, thus decreasing the specific surface

area of all the samples. For the sample synthesized at atmospheric pressure, the pore volume remains constant up to a temperature of 500 °C, which testifies to sintering of its pores by the surface-diffusion mechanism, whereas at an elevation of the calcination temperature to 700–1000 °C sintering proceeds by the volume-diffusion mechanism. Hydrothermal samples are characterized by sintering occurring only by the volume-diffusion mechanism. The thermal stability of the samples is enhanced by the introduction of cerium salt into rutile and its stabilization in the amorphous state in the region of interblock boundaries of TiO_2 crystallites. The stabilizing effect of Ce cations is virtually independent of the rutile synthesis method.

It was shown that the synthesis under severe hydrothermal conditions with a low $[H_2O]/[Ti]$ ratio provides the formation of a more perfect crystal structure of rutile with a small band gap energy (3.00 eV as compared to 3.06 eV for rutile obtained at atmospheric pressure). Differences in the electronic properties may be caused by structural features of the materials (for example, structural defects) or size effects, which are likely to affect their photocatalytic properties.

Acknowledgment

This work was supported by Ministry of Science and Higher Education of the Russian Federation (project AAAA-A17-117041710090-3 for Boreskov Institute of Catalysis).

References

[1]. K. Nakata, A. Fujishima, *J. Photoch. Photobio. C* 13 (2012) 169–189. DOI: 10.1016/j.jphotochemrev.2012.06.001

[2]. P.X. Gao, P. Shimpi, H. Gao, C. Liu, Y. Guo, W. Cai, K.T. Liao, G. Wrobel, Z. Zhang, Z. Ren, H.J. Lin, *Int. J. Mol. Sci.* 13 (2012) 73939–7423. DOI: 10.3390/ijms13067393

[3]. Z. Ren, Y. Guo, C.H. Liu, P.X. Gao, *Front Chem.* 1 (2013) 1–22. DOI: 10.3389/fchem.2013.00018

[4]. F. Mendez-Arriaga, E. de la Calleja, L. Ruiz-Huerta, A. Caballero-Ruiz, R. Almanza, *Mat. Sci. Semicon. Proc.* 100 (2019) 35–41. DOI: 10.1016/j.mssp.2019.04.034

[5]. M.R. Hoffman, S.T. Martin, W. Choi, D.W. Bahnemann, *Chem. Rev.* 95 (1995) 69–96. DOI: 10.1021/cr00033a004

[6]. M. Pelaez, N.T. Nolan, S.C. Pillai, M.K. Seery, P. Falaras, A.G. Kontos, P.S.M. Dunlop, J.W.J. Hamilton, J.A. Byrne, K. O'Shea, M.H. Entezari, D.D. Dionysiou, *Appl. Catal. B: Environ.* 125 (2012) 331–349. DOI: 10.1016/j.apcatb.2012.05.036

[7]. N. Shaham-Waldmann, Y. Paz, *Mat. Sci. Semicon. Proc.* 42 (2016) 72–80. DOI: 10.1016/j.mssp.2015.06.068

[8]. C. Byrne, G. Subramanian, S.C. Pillai, *J. Environ. Chem. Eng.* 6 (2018) 3531–3555. DOI: 10.1016/j.jece.2017.07.080

[9]. A.L. Linsebigler, G. Lu, J.T. Yates, *Chem Rev.* 95 (1995) 735–758. DOI: 10.1021/cr00035a013

[10]. A.J. Haider, Z.N. Jameel, I.H. M. Al-Hussaini, *Energy Procedia* 157 (2019) 17–29. DOI: 10.1016/j.egypro.2018.11.159

[11]. Z. Wu, Q. Wu, L. Du, C. Jiang, L. Piao, *Particuology* 15 (2014) 61–70. DOI: 10.1016/j.partic.2013.04.003

[12]. N.-G. Park, G. Schlichthörl, J. van de Lagemaat, H.M. Cheong, A. Mascarenhas, A.J. Frank, *J. Phys. Chem. B* 103 (1999) 3308–3314. DOI: 10.1021/jp984529i.

[13]. J. Lin, Y-U. Heo, A. Nattestad, Z. Sun, L. Wang, J.H. Kim, S.X. Dou, *Sci. Rep.* 4 (2014) 5769. DOI: 10.1038/srep05769

[14]. Z. Meng, S. Cai, W. Tu, H. Tang, *J. Nanosci. Nanotechnol.* 20 (2020) 1085–1097. DOI: 10.1166/jnn.2020.17325

[15]. R. Khan, S. Javed, M. Islam. Hierarchical Nanostructures of Titanium Dioxide: Synthesis and Applications. In book: Titanium Dioxide-Material for a Sustainable Environment. Edited by D. Yang. BoD-Books on Demand. 2018, 518 p. DOI: 10.5772/intechopen.74525

[16]. Y. Li, Y. Fan, Y. Chen, *J. Mater. Chem.* 12 (2002) 1387–1390. DOI: 10.1039/b2000181

[17]. Z.R. Ismagilov, E.V. Bessudnova, N.V. Shikina, V.A. Ushakov, *Nanotechnol. Russ.* 9 (2014) 21–25. DOI: 10.1134/S1995078014010066

[18]. E.V. Bessudnova, N.V. Shikina, Z.R. Ismagilov, *International Scientific Journal for Alternative Energy and Ecology* [Alternativnaya Energetika i Ekologiya] 7 (147) (2014) 39–47 (in Russ.).

[19]. E.V. Bessudnova, N.V. Shikina, M.S. Mel'gunov, Z.R. Ismagilov, *Nanotechnol. Russ.* 12 (2017) 156–164. DOI: 10.1134/S1995078017020045

[20]. N.V. Shikina, E.V. Bessudnova, A.P. Nikitin, A.V. Ishchenko, N.A. Rudina, D.S. Selishchev, D.V. Kozlov, Z.R. Ismagilov, *J. Nanosci. Nanotechnol.* 20 (2020) 1303–1314. DOI: 10.1166/jnn.2020.16977

[21]. G.A. Zenkovets, A.A. Shutilov, V.Yu. Gavrilov, S.V. Tsybulya, G.N. Kryukova, *Kinet. Catal.* 48 (2007) 742–748. DOI: 10.1134/S0023158407050205

[22]. G.A. Zenkovets, V.Yu. Gavrilov, A.A. Shutilov, S.V. Tsybulya. *Kinet. Catal.* 50 (2009) 760–767. DOI: 10.1134/S002315840905019X

[23]. A.A. Shutilov, G.A. Zenkovets, V.Yu. Gavrilov,

S.V. Tsybulya, *Kinet. Catal.* 52 (2011) 111–118. DOI: 10.1134/S0023158411010174
[24]. N.A. Koryabkina, R.A. Shkrabina, V.A. Ushakov, Z.R. Ismagilov, M. Lausberg, F. Keptein, *Kinet. Catal*. 38 (1997) 112–116.
[25]. N.A. Koryabkina, R.A. Shkrabina, V.A. Ushakov, Z.R. Ismagilov, *Catal. Today* 29 (1996) 427–431. DOI: 10.1016/0920-5861(95)00315-0
[26]. N.V. Shikina, E.V. Bessudnova, V.A. Ushakov, A.P. Nikitin, M.S. Mel'gunov, A.V. Ishchenko, Z. R. Ismagilov, *Nanosystems: Phys. Chem. Math.* 9 (2018) 688–695. DOI: 10.17586/2220-8054-2018-9-5-688-695
[27]. J. Tauc, R. Grigorovici, A. Vancu, *Phys. Stat. Sol.* 15 (1996) 627–637. DOI: 10.1002/pssb.19660150224
[28]. R.L. Penn, J.F. Banfield, *Science* 281 (1998) 969–971. DOI: 10.1126/science.281.5379.969
[29]. T. Zhu, S.P. Gao, *J. Phys. Chem. C* 118 (2014) 11385–11396. DOI: 10.1021/jp412462m
[30]. Y. Cheng, M. Zhang, G. Yao, L. Yang, J. Tao, Z. Gong, G. He, Zhaoqi, Sun, *J. Alloys Compd.* 662 (2016) 179–184. DOI: 10.1016/j.jallcom.2015.12.034
[31]. H. Choi, S. Khan, J. Choi, D.T.T. Dinh, S.Y. Lee, U. Paik, S.-H. Cho, S. Kim, *Appl. Catal. B-Environ.* 210 (2017) 513–521. DOI: 10.1016/j.apcatb.2017.04.020
[32]. H. Lin, C.P. Huang, W. Li, C. Ni, S. Ismat Shah, Yao-Hsuan Tseng, *Appl. Catal. B-Environ.* 68 (2006) 1–11. DOI: 10.1016/j.apcatb.2006.07.018.
[33]. M.E. Contreras-Garcia, M.L. Garcia-Benjume, V.I. Macias-Andres, E. Barajas-Ledesma, A. Medina-Flores, M.I. Espitia-Cabrera, *Mat. Sci. Eng. B* 183 (2014) 78–85. DOI: 10.1016/j.mseb.2014.01.007
[34]. J.C. Cano-Franco, M. Alvarez-Lainez, *Mater. Sci. Semicon. Proc.* 90 (2019) 190–197. DOI: 10.1016/j.mssp.2018.10.017